Photodiagnosis and Photodynamic Therapy 25 (2019) 148–156

Contents lists available at ScienceDirect

Photodiagnosis and Photodynamic Therapy

journal homepage: www.elsevier.com/locate/pdpdt

# Pyropheophorbide-α methyl ester-mediated photodynamic therapy induces apoptosis and inhibits LPS-induced inflammation in RAW264.7 macrophages

Liyi Huang[a], Qing Chen[a], Lehua Yu[b], Dingqun Bai[a,*]

[a] Department of Rehabilitation Medicine, The First Affiliated Hospital of Chongqing Medical University, Chongqing 400016, PR China
[b] Department of Rehabilitation Medicine, The Second Affiliated Hospital of Chongqing Medical University, Chongqing 400010, PR China

ARTICLE INFO

*Keywords:*
MPPa-PDT
RAW264.7
Atherosclerosis
Apoptosis
Inflammation
Photodynamic therapy

ABSTRACT

*Background:* This study aimed to determine the effect of pyropheophorbide-α methyl ester (MPPa)-mediated photodynamic therapy (MPPa-PDT) on the apoptosis and inflammation of murine macrophage RAW264.7 cells.
*Methods:* Uptake and subcellular localization of MPPa was detected by flow cytometry and confocal fluorescence microscope. Cell viability was assessed by CCK-8; ROS levels were assessed by DCFH-DA. Cell apoptosis was measured by flow cytometry and Hoechst 33342 staining, whereas mitochondrial membrane potential was detected by JC-1 staining. Secretion of tumor necrosis factor α (TNF-α), interleukin-1β (IL-1β), and interleukin-6 (IL-6) was determined using ELISA kits. Caspase-3, cleaved caspase-3, procaspase-9, cleaved caspase-9, PARP, cleaved PARP, Bcl-2, Bax, NF-κB p-p65, p-IKKα/β, and p-IκBα were measured by western blotting. Nuclear factor κB (NF-κB)-p65 nuclear translocation was observed by immunofluorescence.
*Results:* MPPa -PDT influenced cell viability in a light dose-dependent manner. It induced ROS formation and RAW264.7 cell apoptosis. It also increased the expression of cleaved caspase-3, cleaved caspase-9, cleaved PARP and Bax, decreased the expression of Bcl-2. While TNF-α, IL-1β, and IL-6 increased in LPS group (model of inflammation), it deceased in LPS-MPPa-PDT group. NF-κB p-p65, p-IKKα/β, and p-IκBα had higher expression in LPS group while that reduced in LPS-MPPa-PDT group. Simultaneously, MPPa-PDT inhibited nuclear translocation of NF-κB-p65 caused by LPS.
*Conclusions:* MPPa-PDT can induce apoptosis and attenuate inflammation in mouse RAW264.7 macrophages, thereby suggesting a promising therapy for atherosclerosis.

## 1. Introduction

Atherosclerosis is a common disease, and acute coronary syndrome (ACS) induced by it is one of the major causes of cardiovascular mortality [1–4]. Atherosclerosis is a chronic systemic multifactorial disease related to oxidative stress and inflammation, which affects all the arterial branches. It is an inflammatory disease that does not result from hypercholesterolemia and lipid accumulation [5]. Macrophages play an indispensable role in the development of atherosclerosis and rupture of the vulnerable plaque. They continue to be the major contributors to inflammatory response through the secretion of pro-inflammatory mediators, such as TNF-α, IL-1β, IL-6, IL-8, MCP-1, and CXC-chemokine ligand 1 (CXCL1). It is increasingly believed that macrophages in plaque are in a dynamic balance, with both macrophage number and inflammatory phenotype influencing plaque fate [6]. Decreasing the infiltration and inflammation of an atherosclerotic plaque with macrophages could stabilize the plaque and inhibit its progression. Therefore, targeting macrophages would be an ideal strategy for identifying and treating vulnerable plaques.

Percutaneous coronary intervention (PCI) is frequently used but has associated sequelae [7]. Statins provide a long-term curative effect on atherosclerosis but are inappropriate for vulnerable plaques. Therefore, it's impending to find a new therapeutic method. Previous studies had demonstrated photodynamic therapy (PDT) to be beneficial to the regression of atherosclerotic plaques [8,9]. PDT is a therapeutic method that combines photosensitizer (PS) with a specific wavelength of light, generating reactive oxygen species (ROS) and causing photochemical reactions [10–12]. Cellular activities of ROS have bidirectional effects that include promotion as well as suppression of inflammation, immunity, and carcinogenesis [13,14]. MPPa is a second-generation photosensitizer, a derivative of chlorophyll that has good absorption at a wavelength of 630 nm [15]. It is a more desirable photosensitizer, for

* Corresponding author.
*E-mail address:* baidingqun2014@163.com (D. Bai).

https://doi.org/10.1016/j.pdpdt.2018.12.002
Received 12 September 2018; Received in revised form 5 November 2018; Accepted 7 December 2018
Available online 15 December 2018
1572-1000/ 

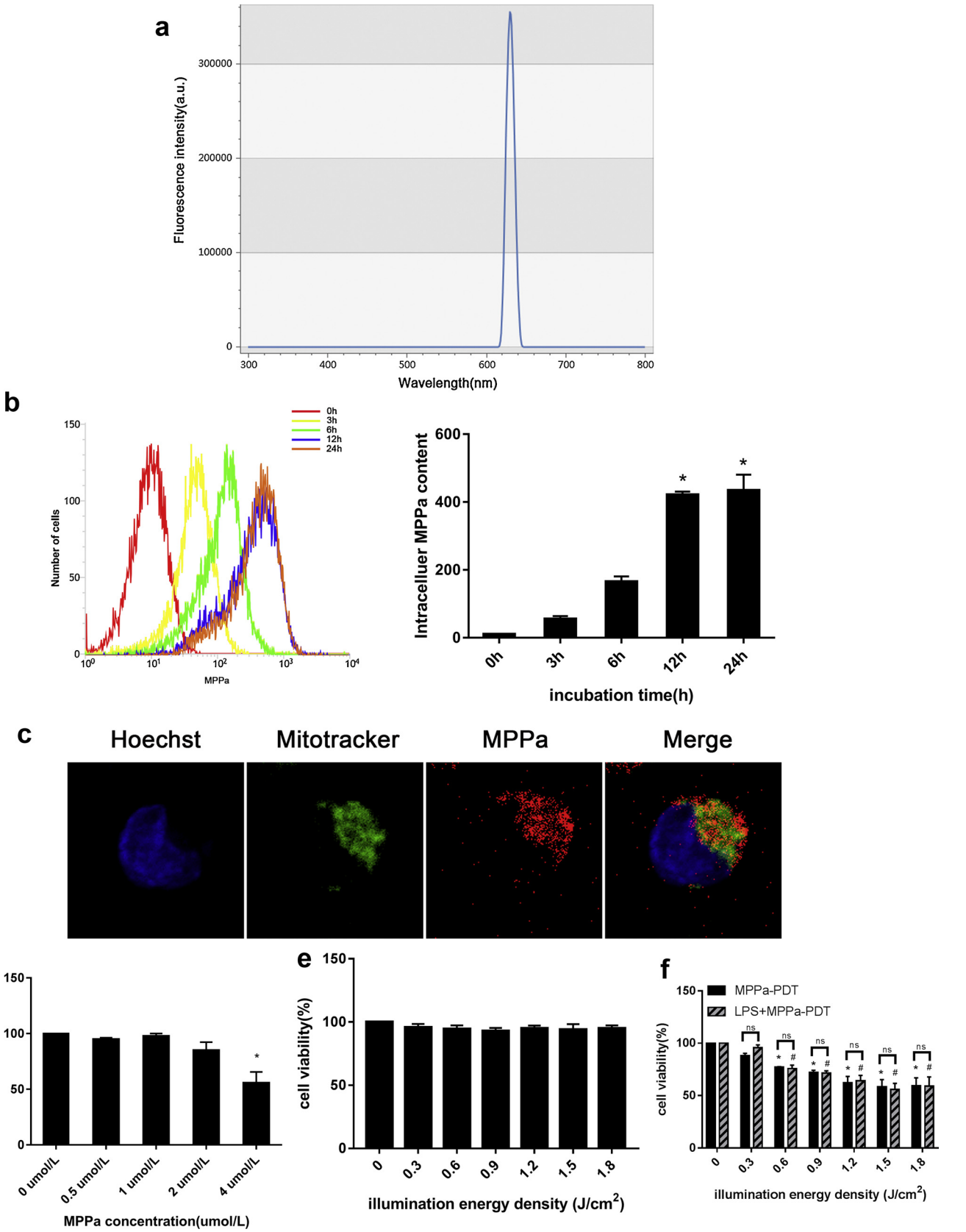


**Fig. 1.** Effect of MPPa-PDT on RAW264.7 cell viability. a MPPa's emission spectrum was observed by Multimode Microplate Reader. b The intracellular MPPa in RAW264.7 macrophages was tested by flow cytometry at different incubation times: 0 h, 3 h, 6 h, 12 h, and 24 h. MPPa increased rapidly during the first 12 h and slowed down during the next 12 h. c MPPa located in mitochondria in RAW264.7 cells (magnification 1200×). d Effect of 0, 0.5, 1, 2, and 4 μmol/L MPPa on RAW264.7 macrophage viability. e Effect of various irradiation energy densities on RAW264.7 macrophage viability. $^{*}P < 0.05$ vs. control group. f Effect of Mppa-PDT on RAW264.7 macrophage viability. Following the incubation with MPPa at 2 μmol/L for 12 h, each cell was irradiated with different energies in presence or absence of LPS, such as 0, 0.3, 0.6, 0.9, 1.2, 1.5, and 1.8 J/cm$^2$. At 24 h post irradiation, cell viabilities were detected by CCK-8 assay. All data shown are mean ± standard error. $^{*}P < 0.05$ vs. control group (MPPa-PDT group), $^{\#}P < 0.05$ vs. control group (LPS + MPPa-PDT group).

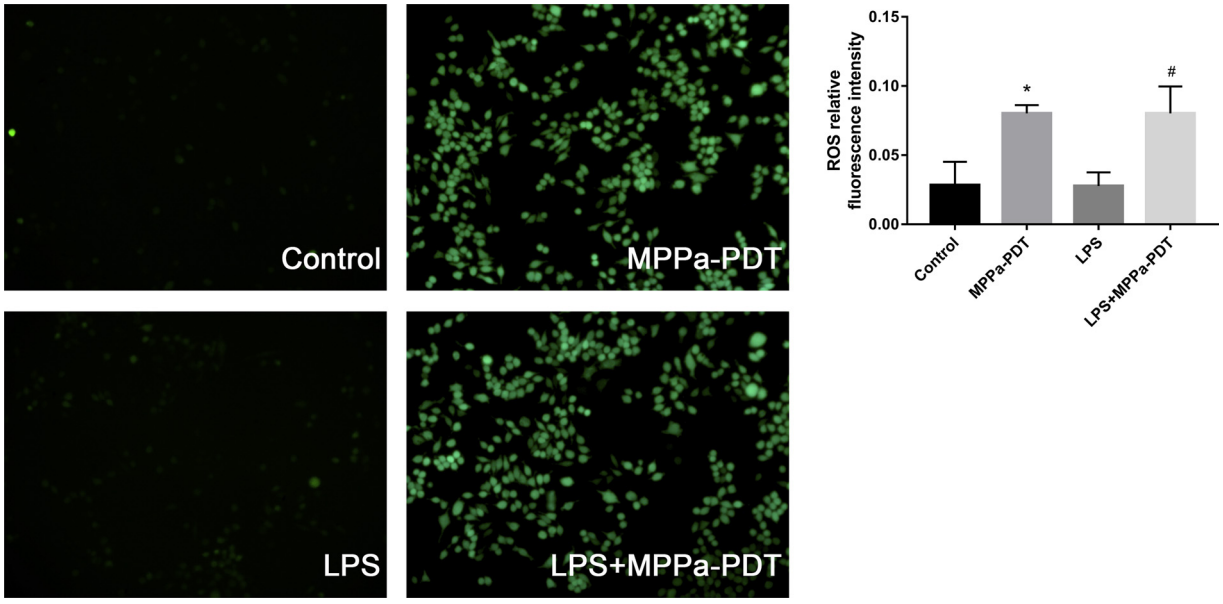


**Fig. 2.** Effect of MPPa-PDT on ROS formation in RAW264.7 macrophages. Following incubation with MPPa at 2 μmol/L for 12 h, cells were irradiated with 0.6 J/cm$^2$, and 100 ng/ml LPS was added after 1 h. Production of ROS was detected under a fluorescence microscope; MPPa-PDT-induced ROS formation, seen in the presence or absence of LPS. (DCFH-DA staining, magnification 200×). All data are mean ± standard error. n = 3 per group. $^*P < 0.05$ vs. control group, $^\#P < 0.05$ vs. LPS group.

better absorbance and stronger permeability, compared to a first-generation photosensitizer [16].

Studies have shown that PDT can eliminate inflammatory cells, repair vessels, promote stability of and reduce plaque [8,9,17,18]. However, the effect of MPPa-mediated PDT on macrophages remains unknown. In the present study, we examined the effect of PDT on LPS-stimulated murine macrophages (RAW264.7).

## 2. Methods

### 2.1. Materials

Pyropheophorbide-α methyl ester (MPPa, $C_{34}H_{36}N_4O_3$) was purchased from Sigma-Aldrich (St Louis, MA). PDT equipment (630 nm, 30 mW/cm$^2$, CW laser) was purchased from Chongqing Jingyu Laser Technology Co., Ltd. (Chongqing, China). Dulbecco's modified Eagle's medium (DMEM) and trypsin were purchased from HyClone (Logan, UT). Fetal bovine serum (FBS) was purchased from PAN-Biotech GmbH (Germany). Lipopolysaccharide (LPS) was obtained from Sigma-Aldrich (St Louis, MA). Cell viability and cytotoxicity test kit (CCK-8) was procured from Dojindo Molecular Technologies (Kumamoto, Japan). Enzyme linked immunosorbent assay kit was purchased from Hangzhou Multi Science (Hangzhou, China). Caspase-3, cleaved caspase-3, caspase-9, PARP, cleaved PARP, Bcl-2, Bax, NF-κB, p-p65, and p-IKKα/β were purchased from Cell Signaling Technology (Danvers, MA), p-IκBα was obtained from Abcam (Cambridge, UK), and β-actin was purchased from Tianjin Sungene Biotech (Tianjin, China). Goat anti-mouse secondary antibody was purchased from Boster Biological Technology (Wuhan, China). JC-1 was purchased from Invitrogen (Paisley, UK), and Hoechst 33342, Antifade Mounting Medium were purchased from Beyotime (Shanghai, China).

### 2.2. Cell culture

The RAW264.7 macrophage line was purchased from Cell Source Center, Chinese Academy of Science (Shanghai, China) and cultured with DMEM (10% FBS) at 37 °C with 5% $CO_2$. DMEM was changed every day or every alternate day. Cells were passaged when they became 70% to 80% confluent.

### 2.3. Detection of intracellular MPPa

MPPa produces red fluorescence upon excitation at a wavelength of 630 nm. MPPa's emission spectrum was determined by Multimode Microplate Reader (Thermo Fisher Scientific, USA). To determine the optimal incubation time of MPPa, we seeded RAW264.7 cells into 6-well plates and incubated for 0 h, 3 h, 6 h, 12 h, and 24 h in the dark, harvested the cells, and washed them with PBS three times. Flow cytometry (BD FACSCalibur, Becton-Dickinson) was employed to measure the intracellular accumulation of MPPa (λexcitation/λemission = 630 nm/631 nm). Cells were incubated with MPPa for 12 h and then upload Mito-Tracker green (Beyotime, Shanghai, China) at a final concentration of 20 nmol/L. And MPPa's location was observed by confocal fluorescence microscope (Nikon A1, Japan).

### 2.4. MPPa-PDT treatment

MPPa was prepared at a concentration of 10 mmol/L and stored in the dark at −80 °C. Working solution was 2 μmol/L as per the previous reports from our research group [12,15]. RAW264.7 macrophages were randomly divided into four groups: Control, MPPa-PDT, LPS, and LPS-MPPa-PDT. Medium of the MPPa-PDT group and LPS + MPPa-PDT group were replaced by medium with 2 μmol/L MPPa after cell attachment; that of control group and LPS group was replaced by isopyknic medium. Cells were cultured in the dark at above-mentioned conditions. After 12 h, MPPa-medium was replaced by fresh medium, same as in control group and LPS group. Then the MPPa-PDT group and LPS + MPPa-PDT group received corresponding irradiations (630 nm, 30 mW/cm$^2$, CW laser) and 100 ng/ml LPS was added to the LPS group and LPS-MPPa-PDT group after 1 h. The cells were cultured in fresh medium for a few hours, and then were subjected to different analyses.

### 2.5. Cell viability and cytotoxicity tests

Cells were seeded in 96-well plates at a density of 5 × 10$^3$ cells/well with three duplicates. The following groups were set: control, MPPa-only, irradiation-only, MPPa-PDT, and LPS + MPPa-PDT. The irradiation-only, MPPa-PDT, and LPS + MPPa-PDT groups were irradiated at a power density of 30 mW/cm$^2$ for the indicated time of 10, 20, 30, 40,

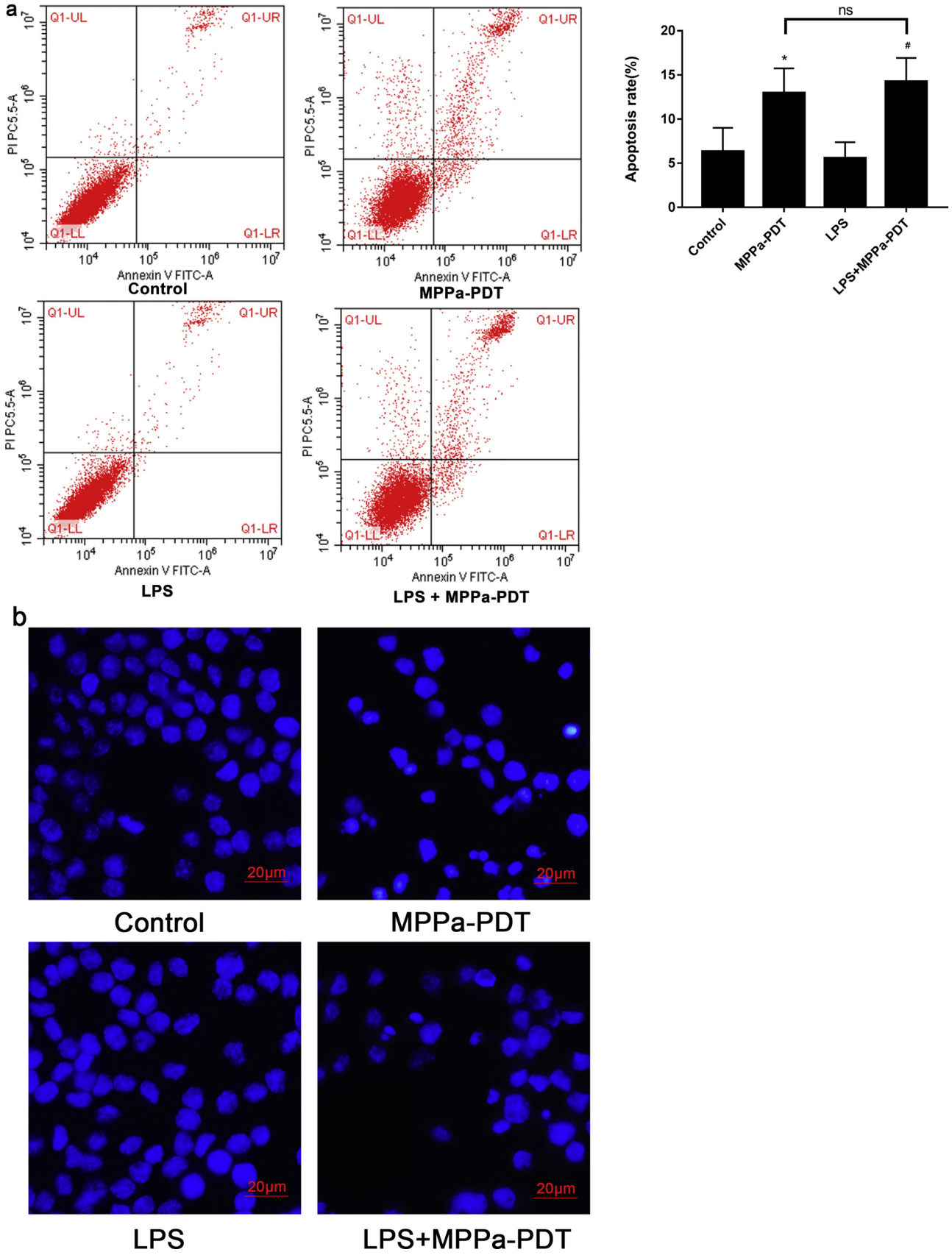


**Fig. 3.** MPPa-PDT induces RAW264.7 cell apoptosis, involved in the mitochondrial apoptosis pathway. Following incubation with MPPa at 2 μmol/L for 12 h, cells were irradiated with 0.6 J/cm$^2$, and 100 ng/ml LPS was added after 1 h; the cells were collected after 12 h. a The cell apoptosis rate was measured by flow cytometry. b Karyopyknosis and fragmentation of RAW264.7 cells were observed under a fluorescence microscope (Hoechst 33342 staining, magnification 400×). c Mitochondrial membrane potential was detected by JC-1 staining (magnification 200×). d Expression of caspase-3, cleaved caspase 3, procaspase-9, and cleaved caspase 9 were measured by western blot. **e** Expressions of cleaved PARP, PARP, Bax, Bcl-2 were measured by western blot. All data are mean ± standard error. n = 3 per group. $^{*}P < 0.05$ vs. control group, $^{\#}P < 0.05$ vs. LPS group.

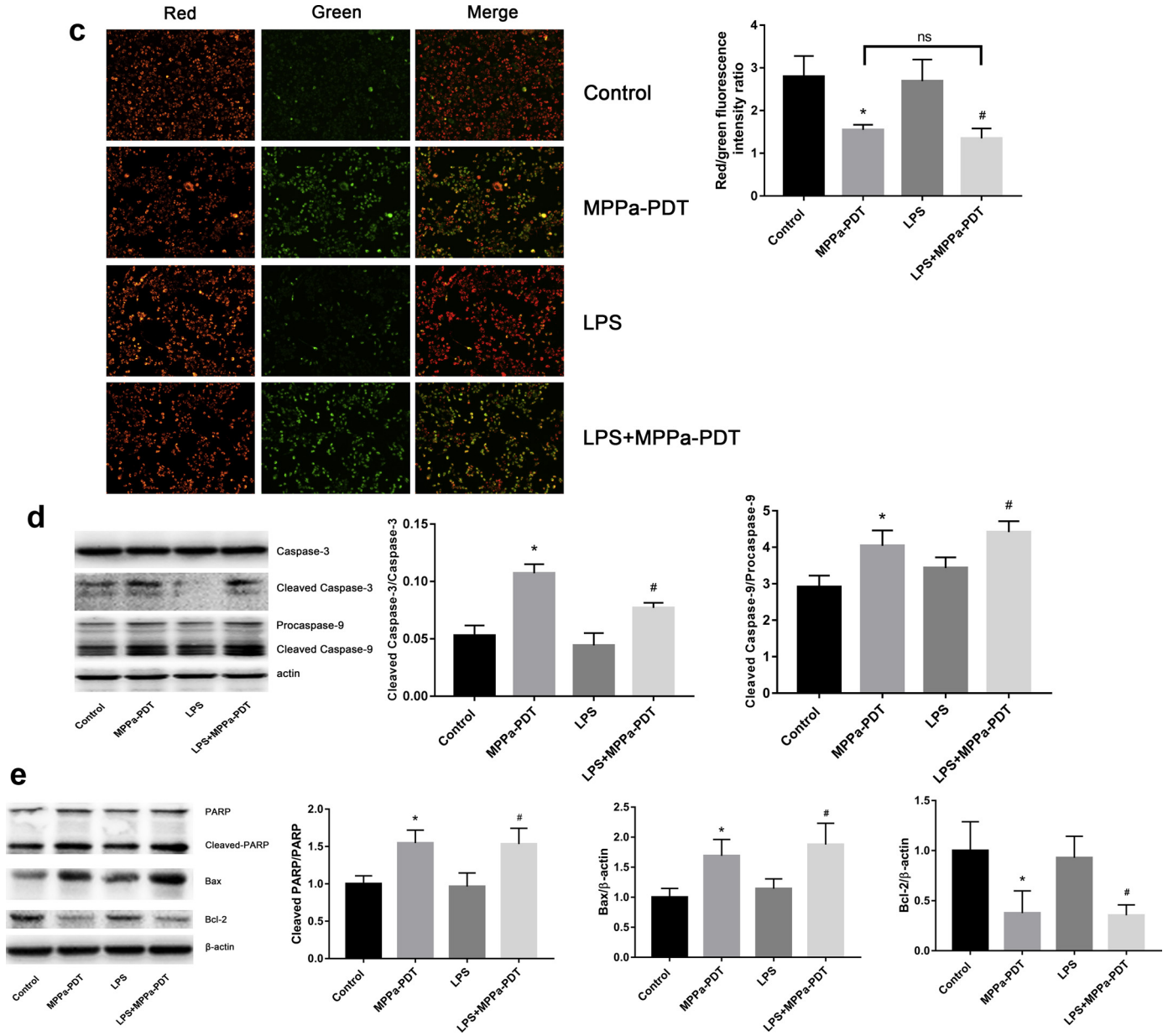


**Fig. 3.** (*continued*)

50, and 60 s (0.3, 0.6, 0.9, 1.2, 1.5, and 1.8 J/cm$^2$, respectively) after replacing the MPPa-medium. After 12 h, 10 microliters of CCK-8 were added to all the wells and further incubated for another 1 h. Microplate reader was used to detect the optical densities (ODs) at a wavelength of 450 nm. Cell viability was calculated by the equation: Cell viability (%) = (Average OD – Average OD of blank group)/(Average OD of control group – Average OD of blank group) × 100%. A blank group containing only DMEM (without cells) was also considered. A sub-lethal dose (0.6 J/cm$^2$) was used for the subsequent studies based on the results. Every group had three duplicates.

### 2.6. ROS detection

RAW264.7 cells were seeded in 24-well plates (5 × 10$^4$ cells/well). DCFH-DA was added to the cells at a concentration of 2 μmol/L after MPPa-PDT and/or LPS treatment, and the cells were incubated for 30 min. Production of ROS was measured under a fluorescence microscope (Zeiss Fluorescence Microscope, Germany).

### 2.7. Determination of cell death by flow cytometry analysis

RAW264.7 cells were inoculated into 6-well plates (1 × 10$^5$ cells/well). All the suspended and adherent cells of the control group, Mppa-PDT group, LPS group, and LPS-Mppa-PDT group were collected at 12 h post treatment, centrifuged at a speed of 1000 r/min and re-suspended with PBS. Subsequently, annexin V and propidium iodide (PI) were added, the mixture was gently agitated, incubated for 15 min at room temperature (25 °C) in the dark, and analyzed by the BD FACSCalibur flow cytometer (BD Biosciences, Franklin Lakes, NJ). Each assay condition was performed in triplicate.

### 2.8. Hoechst nuclear staining

RAW264.7 cells were grown on 24-well plates (5 × 10$^4$ cells/well) over several hours for attachment. Groups and methods were the same as mentioned above. After 12 h, cells were washed thrice with PBS, 3 min each time, and fixed with 4% paraformaldehyde for 20 min. Subsequently, the cells were washed with PBS again and treated with

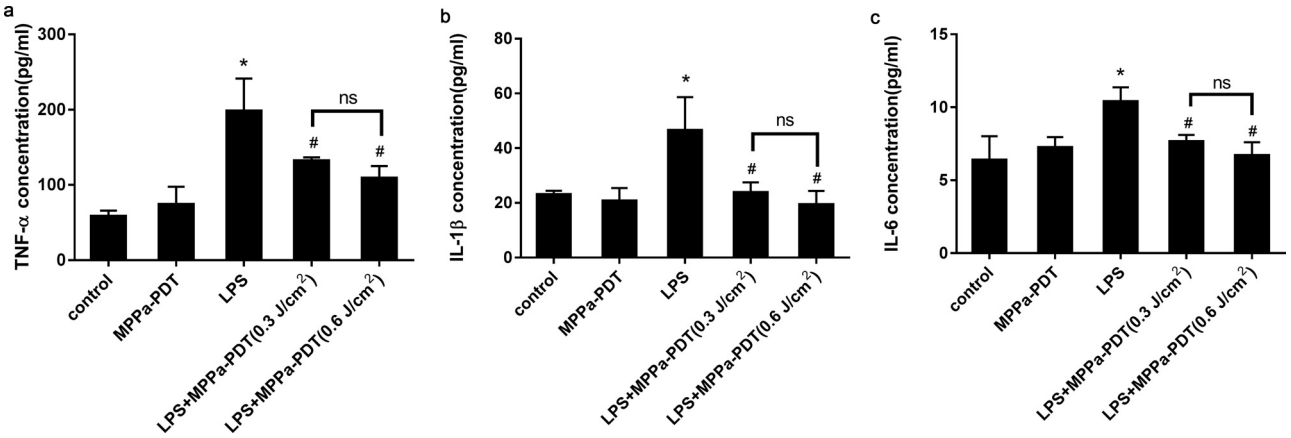


**Fig. 4.** Effect of MPPa-PDT on the expression of inflammatory factors in RAW264.7 macrophages. After diff ;erent treatments, TNF-α, IL-1β, and IL-6, secreted by RAW264.7 macrophages, were measured by ELISA. TNF-α (a), IL-1β (b), and IL-6 (**c**) in LPS groups were significantly higher than in control groups and in MPPa-PDT groups, but MPPa-PDT could reduce the level of these inflammatory factors. All data are mean ± standard error. $^{*}P < 0.05$ vs. Control group, $^{\#}P < 0.05$ vs. LPS group.

0.1% TritonX-100 for 5 min, washed with PBS, and stained with Hoechst 33342 (10 μg/ml) for 20 min, and finally observed under a fluorescence microscope (Leica DMRE Fluorescence Microscope, Germany).

### 2.9. Mitochondrial membrane potential

RAW264.7 cells were grown on 24-well plates ($5 \times 10^4$ cells/well). JC-1 (Invitrogen, Paisley, UK) was added to the cells at 5 μg /ml after treatment. They were incubated for 30 min and membrane potential was measured by fluorescence microscopy (Zeiss Fluorescence Microscope, Germany).

### 2.10. Western blotting

Proteins from RAW264.7 macrophages were collected at 12 h after irradiation. Cells were lysed with RIPA and PMSF, centrifuged at 12,000 g for 15 min at 4 ℃. BCA assay was used to quantify protein concentration. All protein samples used, had the same final concentration and volume. These samples were transferred to PVDF membranes (Millipore) after SDS-PAGE. The membranes were blocked with 5% nonfat dry milk (BIO-RAD) for 2 h at room temperature, washed with Tris-buffered saline containing tween (TBST), and incubated with primary antibodies at 4 ℃ overnight. The membranes were incubated with secondary antibodies and eventually developed by ECL reagent (Beyotime, Shanghai, China). Protein blot images were captured using an imaging densitometer (Fusion FX5, Vilber Lourmat, France). All experiments were triplicated and results were analyzed by Fusion.

### 2.11. Enzyme linked immunosorbent assay (ELISA)

RAW264.7 macrophages were inoculated into 96-well plates ($5 \times 10^3$ cells/well) and incubated overnight for adherence. The control group, MPPa-PDT group, LPS group, and LPS-MPPa-PDT group received different interventions and the cell media were collected at 6 h after irradiation. The levels of inflammatory factors TNF-α, IL-1β, and IL-6 were measured by ELISA, as per the manufacturer's protocol. Every group had triplicates and three experiments were repeated.

### 2.12. Immunofluorescence analysis

RAW264.7 macrophages ($2 \times 10^4$ cells/well) were seeded into 12-well plates that contained glass coverslips. The coverslips were harvested after treatment, washed once with PBS, fixed in 4% paraformaldehyde (PFA) for 20 min, permeabilized with 0.1% Triton-100 for 15 min, washed with PBS, and blocked with 5% BSA for 1 h. Thereafter, the coverslips were incubated with antibodies specific for NF-κB p65 at 4 ℃ overnight. Samples were then incubated with Alexa Fluor 488 goat anti-mouse IgG antibody (Invitrogen) for 1 h, counterstained with Hoechst 33342, and mounted onto slides with Antifade Mounting Medium. The slides were observed under a fluorescence microscope (Leica DMRE Fluorescence Microscope, Germany).

### 2.13. Statistical analysis

Data are presented as mean ± SD. Analyses were carried out using GraphPad Prism Software version 7.00 (San Diego, CA). Diff ;erences among the groups were analyzed using one-way analysis of variance (ANOVA) or SNK-q test. A difference of $P < 0.05$ was considered statistically significant.

## 3. Results

### 3.1. Intracellular intake of MPPa

MPPa's emission spectrum was 631 nm with or without LPS. (Fig. 1a). Quantitative flow cytometry revealed that intracellular MPPa increased with the incubation time. It increased rapidly in the first 12 h and slowed down in the next 12 h (Fig. 1b). Intracellular MPPa showed no significant difference from 12 h to 24 h. Therefore, 12 h was used for subsequent experiments. Confocal fluorescence microscope showed that MPPa localize at mitochondria (Fig. 1c).

### 3.2. Effects of MPPa-PDT on RAW264.7 macrophage viability

In the cell viability assay conducted after MPPa-PDT, low-dose MPPa groups and irradiation-only groups showed no significant difference compared with the control group (incubated with DMEM). However, high-dose of MPPa (4 μmol/L) significantly decreased cell viability (Fig. 1d and e, $P < 0.05$). The results for the MPPa-PDT groups suggested that cell viability was inversely correlated with irradiation dose. LPS had no significant influence on cell viability (Fig. 1f). High-dose MPPa-PDT led to excess ROS generation and induced necrosis in RAW264.7 macrophages, which resulted in the release of a mass of cellular content and inflammatory factors and deterioration of plaques. In this study, we chose a sub-lethal 0.6 J/cm$^2$ as the experimental dose, which yielded a cell viability of 77.39%.

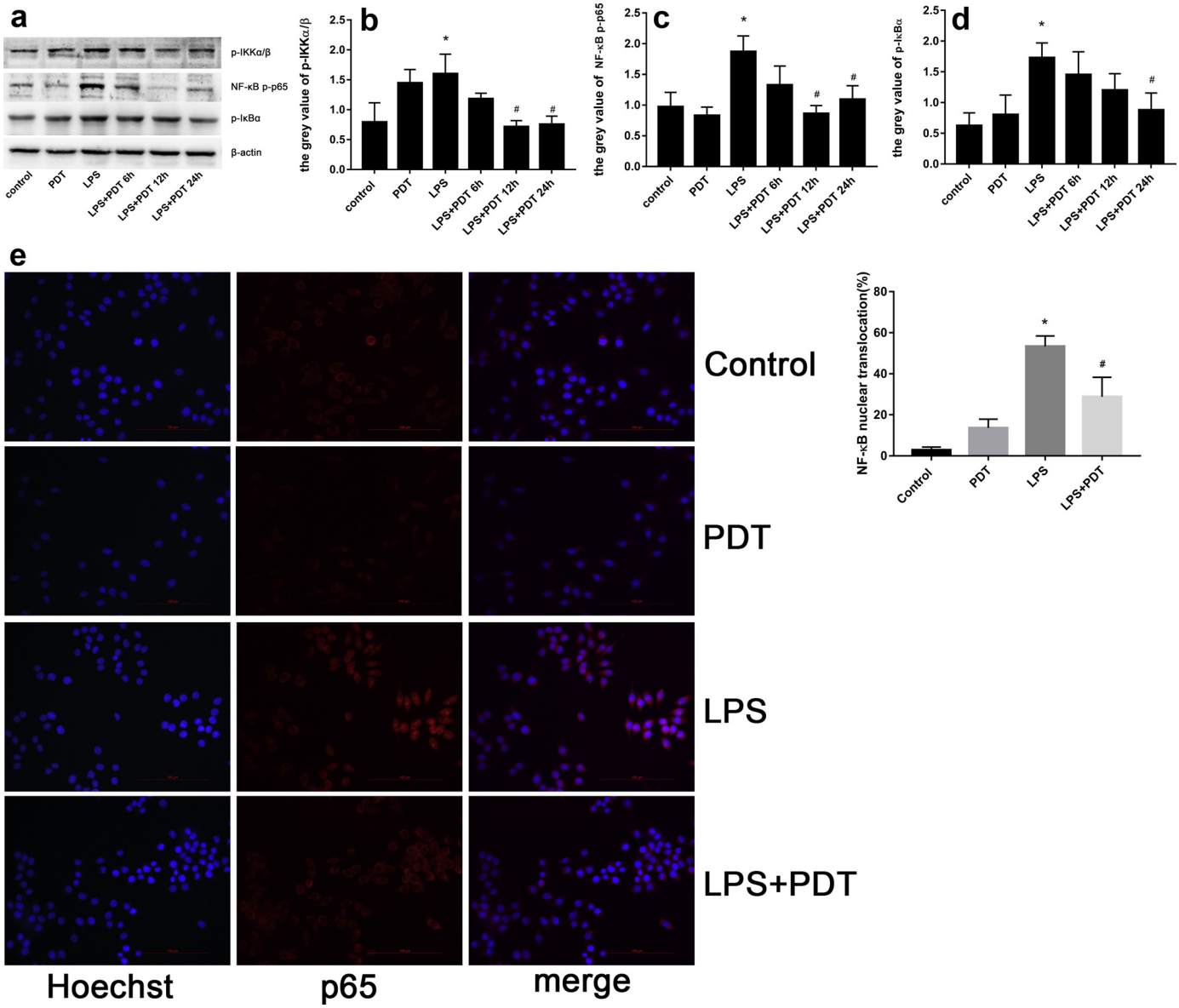


**Fig. 5.** MPPa-PDT decreased the expression level of NF-κB p-p65, p-IKKα/β, and P-IκBα after LPS (a). p-IKKα/β (b), NF-κB p-p65 (c), and P-IκBα (d) were increased after LPS stimulation and decreased after MPPa-PDT. **e** The effect of MPPa-PDT on nuclear translocation of the NF-κB p65 was measured by immunofluorescence. Blue fluorescence represents cell nucleus and red fluorescence represents p65. p65 subunit translocated into the nucleus after LPS stimulation; MPPa-PDT reduced p65 nuclear translocation caused by LPS (scale bar: 100 μm). All data are mean ± standard error. n = 3 per group. $^{*}P < 0.05$ vs. control group, $^{\#}P < 0.05$ vs. LPS group.

### 3.3. Production of ROS

In our experiments, ROS formation was detected after MPPa-PDT. ROS level in the MPPa-PDT group was 2.8 times that in the control group, and ROS level in the LPS + MPPa-PDT was 2.7 times that in the LPS group (Fig. 2). The ROS levels in the control and LPS groups showed no significant difference.

### 3.4. Mechanism of MPPa-PDT-induced apoptosis

Annexin V/PI staining revealed a greater number of apoptotic cells in the MPPa-PDT group than in the control and LPS groups (Fig. 3a). Hoechst nuclear staining also showed that MPPa-PDT induced apoptosis of RAW264.7 cells (Fig. 3b), and there was no significant difference between the control and LPS groups. JC-1 staining demonstrated that the mitochondrial membrane potential was decreased after MPPa-PDT. Cells in the MPPa-PDT and LPS + MPPa-PDT groups had higher green fluorescence intensity, but lower red-to-green fluorescence, than that of the control and LPS groups (Fig. 3c). Cleaved caspase 3 and cleaved caspase 9 were upregulated after MPPa-PDT compared with the control and LPS groups (Fig. 3d). Cleaved PARP and Bax had the parallel tendency while Bcl-2 was downregulated after MPPa-PDT compared with the control and LPS groups (Fig. 3e).

### 3.5. Effect of MPPa-PDT on LPS-induced secretion of inflammatory factors

Quantification of TNF-α, IL-1β, IL-6 revealed that TNF-α levels were significantly higher in the LPS group than in control and MPPa-PDT groups, and the opposite trend was observed for the LPS-MPPa-PDT groups (Fig. 4a, $P < 0.05$). This result indicates that MPPa-PDT inhibited TNF-α secretion. The results for IL-1β and IL-6 were similar to those of TNF-α. There was no significant difference between the control and MPPa-PDT groups ($P > 0.05$).

### 3.6. Effect of MPPa-PDT on inflammation in RAW264.7 macrophages

Changes in NF-κB p-p65, p-IKKα/β, and p-IκBα levels were measured by western blotting, and the results showed that p-IKKα/β was downregulated in the control, MPPa-PDT, and LPS-MPPa-PDT groups, but upregulated in the LPS group (Fig. 5b, $P < 0.05$). For NF-κB p-p65, there was no significant difference between the control and MPPa-PDT groups (Fig. 5c, $P > 0.05$), and it was upregulated in the LPS group and downregulated in the LPS-MPPa-PDT group ($P < 0.05$). P-IκBα was downregulated in the control, MPPa-PDT, and LPS-MPPa-PDT groups and upregulated in the LPS group (Fig. 5d, $P < 0.05$). Immunofluorescence staining for p65 revealed that LPS promoted p65 nuclear translocation but MPPa-PDT reversed this effect (Fig. 5e). Collectively, these results showed that the NF-κB signal pathway maybe involved in the MPPa-PDT-mediated attenuation of macrophage inflammation.

## 4. Discussion

Modern unhealthy lifestyle has increased the incidence of cardiovascular diseases. However, despite rapid advances in treatment modalities and the development of novel cholesterol-lowering drugs, cardiovascular disease due to atherosclerosis remains the primary cause of mortality globally [1,19]. PDT offers several advantages for atherosclerosis. First, photosensitizers can assemble at diseased regions selectively such as atherosclerosis plaques. Spears et al. found that hematoporphyrin derivative (HPD) distributes selectively in the atherosclerotic plaques of erythrocebus patas [18]. To minimize side effects, novel delivery strategies have been developed, such as nanotechnology, liposomes, and intravascular delivery. Second, targeted irradiation of plaques can be realized using optical fiber technology through endovascular light delivery. Third, photosensitizers are activated to trigger responses, including direct killing, effects on vessels, and immune activation, only after stimulation with suitable light. Hayase and his colleagues suggested that PDT can decrease macrophages and atherosclerotic plaque burden without damaging normal vascular walls [20]. Although some environmental problems and technological drawbacks have hindered its routine application for atherosclerosis, such as PSs with low absorption wavelength cannot be activated in the presence of blood and less powerful light delivery devices, the majority of these issues have been resolved. For instance, new-generation PS with longer absorption wavelength can be activated regardless of the interference of blood, and advancements in lasers and light distributors continue to improve light delivery [21].

In this study, we established an inflammatory model by LPS stimulation on the basis of many previous studies that discussed inflammation [22–24]. Cells were treated with 100 ng/ml and 1 μg/ml LPS followed these studies and results showed that 1 μg/ml LPS would influence cells viability (data not show). For this reason, 100 ng/ml LPS was used for consequent experiments. Our results suggested that MPPa accumulation in RAW264.7 macrophages increased with incubation time, indicating that MPPa could distribute selectively in plaques. As we all know, ROS play the most important role in the PDT treatment, thus, we investigate the ROS effects on macrophages. A previous study demonstrated the proinflammatory function of ROS [25]. but ROS exerts bidirectional effects and thus can both promote and suppress inflammation, immune responses, and carcinogenesis. To generate an optimal effect, we examined the effects of various doses of MPPa-PDT in RAW264.7 macrophages, and a sub-lethal dose was chosen for subsequent experiments.

Macrophage proliferation accelerates the formation of vulnerable plaques in atherosclerotic lesions [26]. Thus, their apoptosis is beneficial for decreasing early lesion area in atherosclerosis. Zhu et al. found that UCNPs-Ce6-mediated PDT induced THP-1 macrophage apoptosis via activation of the mitochondrial caspase pathway [27]. Mitochondrial-dependent apoptosis involves the apoptotic protease-activating factor-1 and the formation of an apoptosome, which activates caspase-9 and caspase-3, leading to PARP cleavage and resulting in apoptosis [28]. Our present results are consistent with these reports. Decline of mitochondrial membrane potential, increased expression of cleaved caspase 3/9, cleaved PARP and Bax/Bcl-2 after MPPa-PDT treatment demonstrated that MPPa-PDT induced apoptosis of RAW264.7 cells via the mitochondrial apoptosis pathway.

In atherosclerosis, activation of inflammation can lead to protease secretion, tissue destruction, and plaque rupture [29]. Many factors are involved in atherosclerotic inflammation, such as TNF-α, IL-1β, IL-6, angiotensin-II, IFN-γ, and ICAM-1 [30]. Of these, TNF-α, IL-1β, and IL-6 are implicated in both atherosclerosis and related cardiovascular disease [31,32]. The interaction between these factors facilitates the development and progression of atherosclerosis. Thus, inhibition of these factors is an attractive therapeutic strategy. It is well known that LPS can induce macrophages to differentiate into the inflammatory phenotype via the NF-κB pathway [24]. In this study, TNF-α, IL-1β, and IL-6 levels in the LPS group were higher than those in the control and MPPa-PDT groups. However, the decreased levels in the LPS-MPPa-PDT groups indicated that MPPa-PDT could decrease LPS-stimulated secretion of these factors. Moreover, reduction of the inflammatory factors was not caused by cell death on account of 0.3 $J/cm^2$ didn't affect cellviability significantly. Aleksandra et al. reported that ALA-PDT decreased TNF-α release at 30 $J/cm^2$ but increased it at 10 $J/cm^2$ [33], which indicates that the effects of PDT on inflammatory factors depend on the dose, and the therapy parameters should be selected carefully. PDT has also been reported to inhibit IL-1β secretion by peripheral mononuclear cells [34] Jiang and colleagues demonstrated that HSYA-mediated SDT, which is a method derived from PDT, inhibits inflammation in THP-1 macrophages via suppression of ROS generation.

The IKK/NF-κB signaling pathway exists in nearly all cells and participates in acute and chronic inflammatory responses of mammals. Many researchers believe that NF-κB activation may be the common pathogenetic link among cardiovascular inflammatory diseases [35] and that it might be an important target for atherosclerosis prophylaxis and treatment [36]. In quiescent cells, NF-κB principally resides within the cytoplasm in association with IκB proteins. Following its activation, NF-κB translocate to the nucleus, especially NF-κB P65, and triggers inflammation. In the present study, MPPa-PDT inhibited the LPS-induced expression of p-p65 and nuclear translocation of NF-κB p65, which indicated suppression of the NF-κB signal pathway. These results are comparable with reports on the ability of PDT to attenuate LPS-stimulated increases in NF-κB p50/p65 in macrophages [33]. Kzhyshkowska et al. found that NF-κB could also promote lipid accumulation in macrophage. Recent studies demonstrated that PDT and SDT could induce lipid unloading in macrophages via moderate ROS generation, indicating that these methods might function by suppressing the NF-κB signaling pathway [37–39].

The limitation of the present study is that other signaling pathways that may be involved in the MPPa-PDT-induced inhibition of inflammation in macrophages were not considered. Future studies on MPPa-PDT should investigate the possible involvement of pathways other than NF-κB signaling in the observed effects.

## 5. Conclusion

MPPa-PDT induced apoptosis and inhibited inflammatory responses in macrophages. The present findings may be valuable for the development of novel treatment strategies for atherosclerosis. Further in vivo studies should be performed to develop PDT as a novel treatment for atherosclerosis.

## Conflict of interests

The author(s) confirm that this article content has no conflict of interests . This research did not receive any specific grant from funding

agencies in the public, commercial, or not-for-profit sectors.

## Acknowledgements

The Chongqing Key Laboratory of Translational Medicine in Major Metabolic Diseases, The First Affiliated Hospital of Chongqing Medical University, Chongqing, P.R. China

We would like to thank Editage (www.editage.com) for English language editing.

## References

[1] R. Virmani, A.P. Burke, F.D. Kolodgie, A. Farb, Vulnerable plaque: the pathology of unstable coronary lesions, J. Interv. Cardiol. 15 (6) (2002) 439–446 doi:.

[2] M. Ma, L. Song, H. Yan, M. Liu, L. Zhang, Y. Ma, J. Yuan, J. Hu, Z. Ji, R. Zhang, C. Li, H. Wang, L. Tao, Y. Zhang, Y. Li, Low dose tunicamycin enhances atherosclerotic plaque stability by inducing autophagy, Biochem. Pharmacol. 100 (2016) 51–60, https://doi.org/10.1016/j.bcp.2015.11.020.

[3] P. Zanoni, S.A. Khetarpal, D.B. Larach, W.F. Hancock-Cerutti, J.S. Millar, M. Cuchel, S. DerOhannessian, A. Kontush, P. Surendran, D. Saleheen, S. Trompet, J.W. Jukema, A. De Craen, P. Deloukas, N. Sattar, I. Ford, C. Packard, A. Majumder, D.S. Alam, E. Di Angelantonio, G. Abecasis, R. Chowdhury, J. Erdmann, B.G. Nordestgaard, S.F. Nielsen, A. Tybjaerg-Hansen, R.F. Schmidt, K. Kuulasmaa, D.J. Liu, M. Perola, S. Blankenberg, V. Salomaa, S. Mannisto, P. Amouyel, D. Arveiler, J. Ferrieres, M. Muller-Nurasyid, M. Ferrario, F. Kee, C.J. Willer, N. Samani, H. Schunkert, A.S. Butterworth, J.M. Howson, G.M. Peloso, N.O. Stitziel, J. Danesh, S. Kathiresan, D.J. Rader, Rare variant in scavenger receptor BI raises HDL cholesterol and increases risk of coronary heart disease, Science (New York, N.Y.) 351 (6278) (2016) 1166–1171, https://doi.org/10.1126/science.aad3517.

[4] J. Zhang, S. Yang, X. Ji, Q. Zhou, D. Xing, Characterization of lipid-rich aortic plaques by intravascular photoacoustic tomography: ex vivo and in vivo validation in a rabbit atherosclerosis model with histologic correlation, J. Am. Coll. Cardiol. 64 (4) (2014) 385–390, https://doi.org/10.1016/j.jacc.2014.04.053.

[5] R. Ross, Atherosclerosis–an inflammatory disease, N. Engl. J. Med. 340 (2) (1999) 115–126, https://doi.org/10.1056/nejm199901143400207.

[6] K.J. Moore, F.J. Sheedy, E.A. Fisher, Macrophages in atherosclerosis: a dynamic balance, Nat. Rev. Immunol. 13 (10) (2013) 709–721, https://doi.org/10.1038/nri3520.

[7] P.K. Kuchulakanti, W.W. Chu, R. Torguson, P. Ohlmann, S.W. Rha, L.C. Clavijo, S.W. Kim, A. Bui, N. Gevorkian, Z. Xue, K. Smith, J. Fournadjieva, W.O. Suddath, L.F. Satler, A.D. Pichard, K.M. Kent, R. Waksman, Correlates and long-term outcomes of angiographically proven stent thrombosis with sirolimus- and paclitaxel-eluting stents, Circulation 113 (8) (2006) 1108–1113, https://doi.org/10.1161/CIRCULATIONAHA.105.600155.

[8] R. Waksman, P.E. McEwan, T.I. Moore, R. Pakala, F.D. Kolodgie, D.G. Hellinga, R.C. Seabron, S.J. Rychnovsky, J. Vasek, R.W. Scott, R. Virmani, PhotoPoint photodynamic therapy promotes stabilization of atherosclerotic plaques and inhibits plaque progression, J. Am. Coll. Cardiol. 52 (12) (2008) 1024–1032, https://doi.org/10.1016/j.jacc.2008.06.023.

[9] R. Waksman, I.M. Leitch, J. Roessler, H. Yazdi, R. Seabron, F. Tio, R.W. Scott, R.I. Grove, S. Rychnovsky, B. Robinson, R. Pakala, E. Cheneau, Intracoronary photodynamic therapy reduces neointimal growth without suppressing re-endothelialisation in a porcine model, Heart (Br. Cardiac Soc.) 92 (8) (2006) 1138–1144, https://doi.org/10.1136/hrt.2005.073486.

[10] S. Tian, M. Yong, J. Zhu, L. Zhang, L. Pan, Q. Chen, K.T. Li, Y.H. Kong, Y. Jiang, T.H. Yu, L.H. Yu, D.Q. Bai, Enhancement of the effect of methyl Pyropheophorbide-a-mediated photodynamic therapy was achieved by increasing ROS through inhibition of Nrf2-HO-1 or Nrf2-ABCG2 signaling, Anticancer Agents Med. Chem. 17 (13) (2017) 1824–1836, https://doi.org/10.2174/1871520617666170327145857.

[11] K.-T. Li, Q.-Q. Duan, Q. Chen, J.-W. He, S. Tian, H.-D. Lin, Q. Gao, D.-Q. Bai, The effect of aloe emodin-encapsulated nanoliposome-mediated r-caspase-3 gene transfection and photodynamic therapy on human gastric cancer cells, Cancer Med. 5 (2) (2016) 361–369, https://doi.org/10.1002/cam4.584.

[12] K.T. Li, Q. Chen, D.W. Wang, Q.Q. Duan, S. Tian, J.W. He, Y.S. Ou, D.Q. Bai, Mitochondrial pathway and endoplasmic reticulum stress participate in the photosensitizing effectiveness of AE-PDT in MG63 cells, Cancer Med. 5 (11) (2016) 3186–3193, https://doi.org/10.1002/cam4.895.

[13] C. Nathan, A. Cunningham-Bussel, Beyond oxidative stress: an immunologist's guide to reactive oxygen species, Nat. Rev. Immunol. 13 (5) (2013) 349–361, https://doi.org/10.1038/nri3423.

[14] M. Broekgaarden, R. Weijer, T.M. van Gulik, M.R. Hamblin, M. Heger, Tumor cell survival pathways activated by photodynamic therapy: a molecular basis for pharmacological inhibition strategies, Cancer Metastasis Rev. 34 (4) (2015) 643–690, https://doi.org/10.1007/s10555-015-9588-7.

[15] L. Pan, H. Lin, S. Tian, D. Bai, Y. Kong, L. Yu, The sensitivity of glioma cells to pyropheophorbide-alphamethyl ester-mediated photodynamic therapy is enhanced by inhibiting ABCG2, Lasers Surg. Med. 49 (7) (2017) 719–726, https://doi.org/10.1002/lsm.22661.

[16] I. Yoon, J.Z. Li, Y.K. Shim, Advance in photosensitizers and light delivery for photodynamic therapy, Clin. Endosc. 46 (1) (2013) 7–23, https://doi.org/10.5946/ce.2013.46.1.7.

[17] C. Peng, Y. Li, H. Liang, J. Cheng, Q. Li, X. Sun, Z. Li, F. Wang, Y. Guo, Z. Tian, L. Yang, Y. Tian, Z. Zhang, W. Cao, Detection and photodynamic therapy of inflamed atherosclerotic plaques in the carotid artery of rabbits, J. Photochem. Photobiol. B, Biol. 102 (1) (2011) 26–31, https://doi.org/10.1016/j.jphotobiol.2010.09.001.

[18] J.R. Spears, J. Serur, D. Shropshire, S. Paulin, Fluorescence of experimental atheromatous plaques with hematoporphyrin derivative, J. Clin. Invest. 71 (2) (1983) 395–399 doi:.

[19] W.E. Hellings, W. Peeters, F.L. Moll, G. Pasterkamp, From vulnerable plaque to vulnerable patient: the search for biomarkers of plaque destabilization, Trends Cardiovasc. Med. 17 (5) (2007) 162–171, https://doi.org/10.1016/j.tcm.2007.03.006.

[20] M. Hayase, K.W. Woodburn, J. Perlroth, R.A. Miller, W. Baumgardner, P.G. Yock, A. Yeung, Photoangioplasty with local motexafin lutetium delivery reduces macrophages in a rabbit post-balloon injury model, Cardiovasc. Res. 49 (2) (2001) 449–455 doi:.

[21] M. Jain, M. Zellweger, G. Wagnières, H. van den Bergh, S. Cook, M.-N. Giraud, Photodynamic therapy for the treatment of atherosclerotic plaque: lost in translation? Cardiovasc. Ther. 35 (2) (2017) e12238, https://doi.org/10.1111/1755-5922.12238.

[22] Y.P. Zeng, C. Yang, Y. Li, Y. Fan, H.J. Yang, B. Liu, H.X. Sang, Aspirin inhibits osteoclastogenesis by suppressing the activation of NF-kappaB and MAPKs in RANKL-induced RAW264.7 cells, Mol. Med. Rep. 14 (3) (2016) 1957–1962, https://doi.org/10.3892/mmr.2016.5456.

[23] S. Ahn, P. Singh, M. Jang, Y.J. Kim, V. Castro-Aceituno, S.Y. Simu, Y.J. Kim, D.C. Yang, Gold nanoflowers synthesized using Acanthopanacis cortex extract inhibit inflammatory mediators in LPS-induced RAW264.7 macrophages via NF-kappaB and AP-1 pathways, Colloids Surf. B, Biointerfaces 160 (2017) 423–428, https://doi.org/10.1016/j.colsurfb.2017.09.053 doi:.

[24] H. Zhang, Y. Shan, Y. Wu, C. Xu, X. Yu, J. Zhao, J. Yan, W. Shang, Berberine suppresses LPS-induced inflammation through modulating Sirt1/NF-kappaB signaling pathway in RAW264.7 cells, Int. Immunopharmacol. 52 (2017) 93–100, https://doi.org/10.1016/j.intimp.2017.08.032.

[25] I.T. Lee, C.M. Yang, Role of NADPH oxidase/ROS in pro-inflammatory mediators-induced airway and pulmonary diseases, Biochem. Pharmacol. 84 (5) (2012) 581–590, https://doi.org/10.1016/j.bcp.2012.05.005.

[26] X. Zheng, J. Wu, Q. Shao, X. Li, J. Kou, X. Zhu, Z. Zhong, Y. Jiang, Z. Liu, H. Li, Y. Tian, L. Yang, Apoptosis of THP-1 macrophages induced by pseudohypericin-mediated sonodynamic therapy through the mitochondria-caspase pathway, Cell. Physiol. Biochem. 38 (2) (2016) 545–557, https://doi.org/10.1159/000438649 doi:.

[27] X. Zhu, H. Wang, L. Zheng, Z. Zhong, X. Li, J. Zhao, J. Kou, Y. Jiang, X. Zheng, Z. Liu, H. Li, W. Cao, Y. Tian, Y. Wang, L. Yang, Upconversion nanoparticle-mediated photodynamic therapy induces THP-1 macrophage apoptosis via ROS bursts and activation of the mitochondrial caspase pathway, Int. J. Nanomed. 10 (2015) 3719–3736, https://doi.org/10.2147/ijn.s82162.

[28] G. van Loo, X. Saelens, M. van Gurp, M. MacFarlane, S.J. Martin, P. Vandenabeele, The role of mitochondrial factors in apoptosis: a Russian roulette with more than one bullet, Cell Death Differ. 9 (10) (2002) 1031–1042, https://doi.org/10.1038/sj.cdd.4401088.

[29] Y. Jiang, J. Kou, X. Han, X. Li, Z. Zhong, Z. Liu, Y. Zheng, Y. Tian, L. Yang, ROS-dependent activation of autophagy through the PI3K/Akt/mTOR pathway is induced by hydroxysafflor yellow A-Sonodynamic therapy in THP-1 macrophages, Oxid. Med. Cell. Longev. 2017 (2017) 8519169, https://doi.org/10.1155/2017/8519169.

[30] D. Tousoulis, A.M. Kampoli, N. Papageorgiou, E. Androulakis, C. Antoniades, K. Toutouzas, C. Stefanadis, Pathophysiology of atherosclerosis: the role of inflammation, Curr. Pharm. Des. 17 (37) (2011) 4089–4110 doi:.

[31] J. Kzhyshkowska, C. Neyen, S. Gordon, Role of macrophage scavenger receptors in atherosclerosis, Immunobiology 217 (5) (2012) 492–502, https://doi.org/10.1016/j.imbio.2012.02.015.

[32] D. Tousoulis, G. Davies, C. Stefanadis, P. Toutouzas, J.A. Ambrose, Inflammatory and thrombotic mechanisms in coronary atherosclerosis, Heart (British Cardiac Society) 89 (9) (2003) 993–997 doi:.

[33] A. Kawczyk-Krupka, Z. Czuba, E. Szliszka, W. Krol, A. Sieron, The role of photosensitized macrophages in photodynamic therapy, Oncol. Rep. 26 (1) (2011) 275–280, https://doi.org/10.3892/or.2011.1262.

[34] W.H. Boehncke, K. Konig, R. Kaufmann, W. Scheffold, O. Prummer, W. Sterry, Photodynamic therapy in psoriasis: suppression of cytokine production in vitro and recording of fluorescence modification during treatment in vivo, Arch. Dermatol. Res. 286 (6) (1994) 300–303 doi:.

[35] M. Halle, P. Hall, P. Tornvall, Cardiovascular disease associated with radiotherapy: activation of nuclear factor kappa-B, J. Intern. Med. 269 (5) (2011) 469–477, https://doi.org/10.1111/j.1365-2796.2011.02353.x.

[36] G.J. Zhao, K. Yin, Y.C. Fu, C.K. Tang, The interaction of ApoA-I and ABCA1 triggers signal transduction pathways to mediate efflux of cellular lipids, Mol. Med. (Cambridge, Mass) 18 (2012) 149–158, https://doi.org/10.2119/molmed.2011.00183.

[37] F. Tian, J. Yao, M. Yan, X. Sun, W. Wang, W. Gao, Z. Tian, S. Guo, Z. Dong, B. Li, T. Gao, P. Shan, B. Liu, H. Wang, J. Cheng, Q. Gao, Z. Zhang, W. Cao, Y. Tian, 5-aminolevulinic acid-mediated sonodynamic therapy inhibits RIPK1/RIPK3-dependent necroptosis in THP-1-Derived foam cells, Sci. Rep. 6 (2016) 21992, https://doi.org/10.1038/srep21992.

[38] X. Li, X. Zhang, L. Zheng, J. Kou, Z. Zhong, Y. Jiang, W. Wang, Z. Dong, Z. Liu, X. Han, J. Li, Y. Tian, Y. Zhao, L. Yang, Hypericin-mediated sonodynamic therapy induces autophagy and decreases lipids in THP-1 macrophage by promoting ROS-dependent nuclear translocation of TFEB, Cell Death Dis. 7 (12) (2016) e2527, https://doi.org/10.1038/cddis.2016.433.

[39] J.Y. Kou, Y. Li, Z.Y. Zhong, Y.Q. Jiang, X.S. Li, X.B. Han, Z.N. Liu, Y. Tian, L.M. Yang, Berberine-sonodynamic therapy induces autophagy and lipid unloading in macrophage, Cell Death Dis. 8 (1) (2017) e2558, https://doi.org/10.1038/cddis.2016.354.